ACS Medicinal Chemistry Letters

Letter

pubs.acs.org/acsmedchemlett

Evaluation of [^{11}C]*N*-Methyl Lansoprazole as a Radiopharmaceutical for PET Imaging of Tau Neurofibrillary Tangles

Xia Shao,[†] Garrett M. Carpenter,[†] Timothy J. Desmond,[†] Phillip Sherman,[†] Carole A. Quesada,[†] Maria Fawaz,[†] Allen F. Brooks,[†] Michael R. Kilbourn,[†] Roger L. Albin,[‡,§] Kirk A. Frey,[†,§] and Peter J. H. Scott*[,†,∥]

[†]Division of Nuclear Medicine, Department of Radiology, The University of Michigan Medical School, Ann Arbor, Michigan 48109, United States

[‡]Geriatrics Research, Education, and Clinical Center, VAAAHS, Ann Arbor, Michigan 48105, United States

[§]Department of Neurology, The University of Michigan Medical School, Ann Arbor, Michigan 48109, United States

[∥]The Interdepartmental Program in Medicinal Chemistry, The University of Michigan, Ann Arbor, Michigan 48109, United States

Supporting Information

ABSTRACT: [^{11}C]*N*-Methyl lansoprazole ([^{11}C]NML, **3**) was synthesized and evaluated as a radiopharmaceutical for quantifying tau neurofibrillary tangle (NFT) burden using positron emission tomography (PET) imaging. [^{11}C]NML was synthesized from commercially available lansoprazole in 4.6% radiochemical yield (noncorrected RCY, based upon [^{11}C]MeI), 99% radiochemical purity, and 16095 Ci/mmol specific activity (n = 5). Log P was determined to be 2.18. A lack of brain uptake in rodent microPET imaging revealed [^{11}C]NML to be a substrate for the rodent permeability-glycoprotein 1 (PGP) transporter, but this could be overcome by pretreating with cyclosporin A to block the PGP. Contrastingly, [^{11}C]NML was not found to be a substrate for the primate PGP, and microPET imaging in rhesus revealed [^{11}C]NML uptake in the healthy primate brain of ∼1600 nCi/cc maximum at 3 min followed by rapid egress to 500 nCi/cc. Comparative autoradiography between wild-type rats and transgenic rats expressing human tau (hTau +/+) revealed 12% higher uptake of [^{11}C]NML in the cortex of brains expressing human tau. Further autoradiography with tau positive brain samples from progressive supranuclear palsy (PSP) patients revealed colocalization of [^{11}C]NML with tau NFTs identified using modified Bielschowsky staining. Finally, saturation binding experiments with heparin-induced tau confirmed K_d and Bmax values of [^{11}C]NML as 700 pM and 0.214 fmol/μg, respectively.

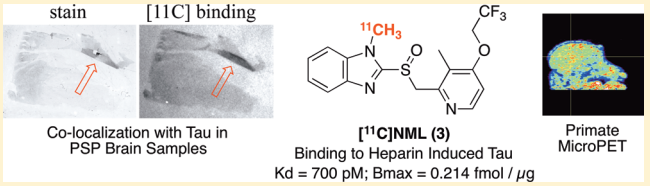

KEYWORDS: *Alzheimer's disease, tauopathies, neuroimaging, positron emission tomography imaging, carbon-11*

Dementia is estimated to effect 14000/100000 of the population, 5% over the age of 70 and 24% over the age of 80.[1] The most common form is Alzheimer's disease (AD), accounting for 50% of the dementia landscape, and at the time of writing, over 5 million cases were in the United States alone. AD is characterized by the presence of both extracellular senile plaques composed of β-amyloid (Aβ) and intracellular neurofibrillary tangles (NFTs) made up of aggregated tau protein.[2] Additional decline of neurotransmitter systems such as the cholinergic system occurs concurrently.[3]

Significant work has been undertaken to develop radiopharmaceuticals that allow noninvasive imaging of dementias such as AD using positron emission tomography (PET) imaging.[4] The goals of imaging AD pathophysiology with PET are (a) diagnosis of the condition (historically achieved postmortem) while the patient is still alive and, ideally, before the onset of cognitive decline; (b) differentiation of clinically overlapping dementia subtypes enabling appropriate clinical management (current clinical accuracy is ∼60−80%); (c) selection of appropriate patients for clinical trials of AD therapeutics; and (d) monitoring patient response to such therapeutics.

The most commonly explored strategy to date involves imaging of senile amyloid plaques (recently reviewed[4−8]) because, for decades, the presence of senile plaques has been the definitive diagnosis of AD. Moreover, the amyloid hypothesis suggested that amyloid plaque burden correlated with cognitive decline.[9,10] Thus, [^{11}C]PiB (University of Pittsburgh),[11] [^{18}F]flutemetamol (GE Healthcare),[12] [^{18}F]-amyvid ([^{18}F]florbetapir, Avid Radiopharmaceuticals/Eli Lilly),[13] and [^{18}F]florbetaben (Bayer Healthcare/Piramal Healthcare)[14] have all been extensively developed. These compounds all show high cortical uptake in amyloid-positive patients but are hampered by nonspecific white matter binding, even in amyloid-negative patients.[15] Proof-of-mechanism has also been confirmed by pivotal autopsy studies.[16,17] [^{18}F]-Amyvid was the first of these to garner marketing approval from

Special Issue: Alzheimer's Disease

Received: July 30, 2012
Accepted: September 25, 2012
Published: September 25, 2012

the U.S. FDA, in April 2012, as a radioactive diagnostic agent for PET imaging of the brain to estimate Aβ neuritic plaque density in adults. These agents are expected to be crucial if an antiamyloid therapeutic strategy is identified.

However, as more than one neurodegenerative disorder is associated with amyloid pathology [e.g., AD and dementia with Lewy bodies (DLB)], amyloid imaging alone is not sufficient to differentiate dementia subtypes. Moreover, it has been shown that extracellular amyloid does not correlate with cognitive status [estimated using the minimental state examination (MMSE)] in AD.[18] Contrastingly, in the same work, Hof and co-workers demonstrated that intracellular tau NFT burden does correlate with cognitive decline, confirming tau NFTs as a viable target for AD therapy and PET imaging of AD. Furthermore, tau NFTs are implicated in numerous other dementia subtypes. These tauopathies include frontotemporal dementia (FTD), progressive supranuclear palsy (PSP), and corticobasal degeneration (CBD).[19] Therefore, in addition to AD, a radiopharmaceutical for quantifying tau NFT burden would aid in the understanding of the pathophysiology and clinical management of each of these neurodegenerative conditions.

Despite this, the development of radiopharmaceuticals for tau NFTs has been comparatively limited, and those there are remain mostly confined to the preclinical arena. Okamura and colleagues screened >2000 compounds against tau and identified quinolines and benzimidazoles as scaffolds of interest.[20] A number of groups have explored the quinoline scaffold, and both [^{11}C]BF156[20] and [^{18}F]THK523[21] appear to have affinity for tau and specificity for tau over Aβ, although preliminary clinical imaging with [^{18}F]THK523 was unable to distinguish AD patients from healthy controls.[22] Other radiopharmaceuticals for tau include [^{18}F]T808[23] and [^{18}F]-FDDNP,[24] although utility of the latter compound is hampered by its affinity for both tau and Aβ.

At the University of Michigan, we have an extremely active neuroimaging program and are interested in having the ability to image tau NFTs. Reflecting this, we were attracted by a report from Rojo and colleagues in 2010, which indicated that lansoprazole, an FDA-approved proton pump inhibitor, has nanomolar affinity for certain forms of tau and specificity for tau over amyloid.[25] As lansoprazole (**1**) contains a benzoimidazole, this would appear to be in line with Okamura's findings.[20] Herein, we report the synthesis and preliminary preclinical evaluation of [^{11}C]*N*-methyl lansoprazole ([^{11}C]NML, **3**).

When considering how to synthesize a radiolabeled analogue of lansoprazole (Scheme 1), it was apparent to us that the benzoimidazole moiety was readily amenable to methylation with [^{11}C]MeOTf, using standard carbon-11 radiochemical techniques routinely employed in our laboratory.[26] The identity and purity of a radiopharmaceutical are confirmed via coinjection of the radiolabeled compound and a sample of unlabeled reference standard onto an analytical HPLC. A reference standard (**2**) was synthesized in 58% yield from commercially available lansoprazole (**1**) by treatment with methyl iodide and characterized by NMR, HRMS, and HPLC, which agreed with literature values.[27] With reference standard in hand, we proceeded with radiolabeling. A thin film of lansoprazole (**1**), dissolved in THF, was deposited onto the HPLC loop of a TRACERlab FXc-pro carbon-11 synthesis module. [^{11}C]MeOTf was then passed through the loop for 5 min to generate [^{11}C]NML (**3**), which was purified by

Scheme 1. Synthesis of [^{11}C]NML and Reference Standard[a]

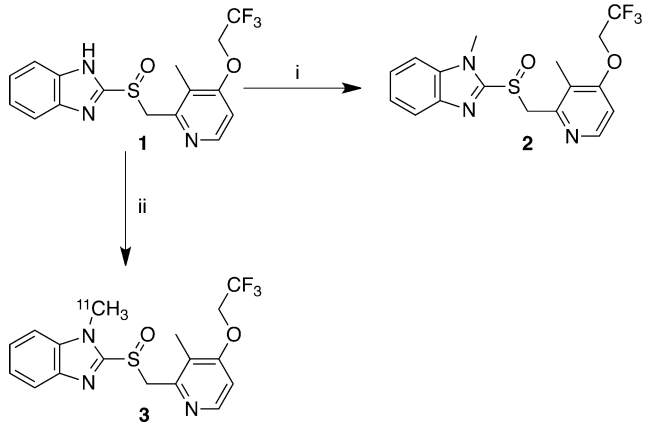

[a]Reagents and conditions: (i) MeI, KOH, water, 60 °C, 10 min, 58%. (ii) [^{11}C]MeOTf, 5 min [loop chemistry], semipreparative HPLC, SPE, 4.6% RCY.

semipreparative HPLC. Subsequent reconstitution of the HPLC fraction into ethanolic saline provided doses of [^{11}C]NML [4.6% nondecay-corrected radiochemical yield based upon [^{11}C]MeI (the precursor to [^{11}C]MeOTf), 99% radiochemical purity, specific activity = 16095 Ci/mmol, n = 5] suitable for preclinical evaluation (and eventual human use).

Rojo and colleagues reported the log *P* value of lansoprazole to be 1.47[25] (although a range of ∼1.5−2.76, often attributed to pH dependency, is apparent). Regardless of the literature variability, excellent CNS permeability is expected for compounds with log *P* values in this range. The *N*-methyl analogue synthesized herein was expected to have a slightly higher log *P* than the parent due to the additional methyl group, and indeed, we determined log $P_{octanol/water}$ to be 2.18. This makes [^{11}C]NML slightly more polar than [^{11}C]PiB and definitely suitable as a radiopharmaceutical for use in the CNS.

With these data in hand, we conducted [^{11}C]NML microPET in rodents (n = 2) to evaluate brain kinetics of the new radiopharmaceutical. To our surprise, there was minimal brain uptake of [^{11}C]NML in the baseline rodent scans (Figure 1). This lack of brain uptake was also confirmed by ex vivo biodistribution studies conducted at 5, 30, and 60 min (n = 3 at each time point, see the Supporting Information). Initially, we suspected that we had not made compounds **2** and **3**. Erroneous methylation of the pyridine, while unfavored as

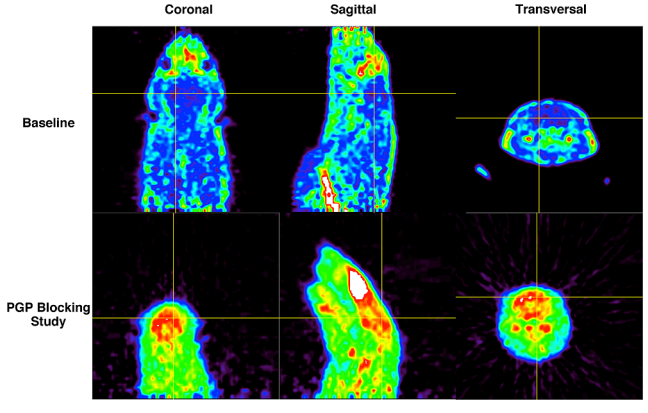

Figure 1. Rodent microPET images.

dx.doi.org/10.1021/ml300216t | ACS Med. Chem. Lett. 2012, 3, 936−941

compared to methylation of the benzoimidazole, could lead to the observed result. Methylation of the pyridine would provide pyridinium salt **4**, a compound expected to appear similar to **2** by mass spectrometry and NMR spectroscopy, which, as a charged species, would be unlikely to cross the blood−brain barrier (BBB). However, careful reanalysis of the mass spectra of compound **2** revealed fragments **5** (M + H = 133) and **6** (M + H = 252) but not fragments **7** or **8**, confirming that we had indeed prepared the intended *N*-methyl derivative **2** (Scheme 2).

Scheme 2. Mass Spectroscopy of Reference Standard 2

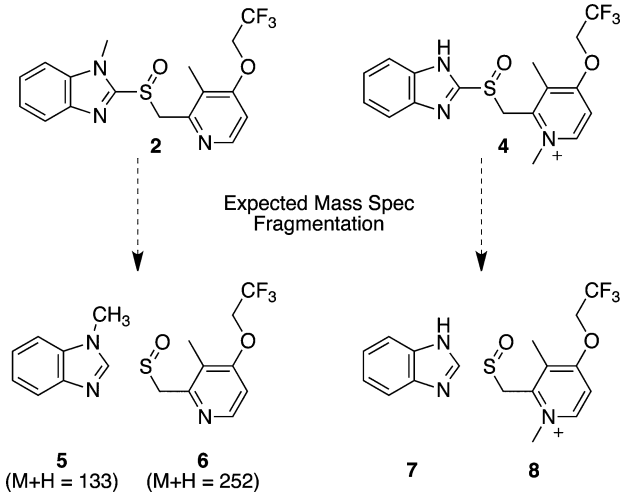

The analytical data and favorable log *P* all suggested that [^{11}C]NML should cross the BBB and enter the CNS. We therefore considered alternative explanations for the lack of brain uptake, and one possibility was transporter involvement as there are a number of active transporters on the BBB. If [^{11}C]NML was a substrate for one of these, then it could be transported out of the brain and lead to the appearance of no brain uptake on the microPET scans. The most likely culprit was the permeability-glycoprotein 1 [PGP, or multidrug resistance protein 1 (MDR1)], found in many locations in the body including the BBB. PGP is a well-known ATP-binding cassette transporter that can transport a wide range of molecules across both intra- and extracellular membranes.[28] To test this hypothesis, rodent microPET imaging was repeated in the presence of cyclosporin A, an immunosuppressant drug known to block PGP activity.[29] The resulting PET scans (Figure 1) showed the expected higher levels of brain uptake of [^{11}C]NML, confirming our hypothesis.

Lack of brain uptake would ordinarily obviate terminating development of [^{11}C]NML as a radiopharmaceutical for quantifying tau NFT burden. However, cognizant of frequent differences in drug pharmacology and pharmacokinetics between species, we were curious about how [^{11}C]NML would behave in our primates. Having the luxury of drug naïve rhesus monkeys available exclusively for use in microPET developmental work, we conducted nonhuman primate microPET imaging (Figure 2A) with [^{11}C]NML. Our notion about species variation proved to be the case, and [^{11}C]NML appears to be a substrate for the rodent PGP transporter but not the corresponding primate PGP transporter. Our expectation is that the pharmacology and pharmacokinetics of [^{11}C]NML in humans will more closely resemble that of the nonhuman primates than rodents.

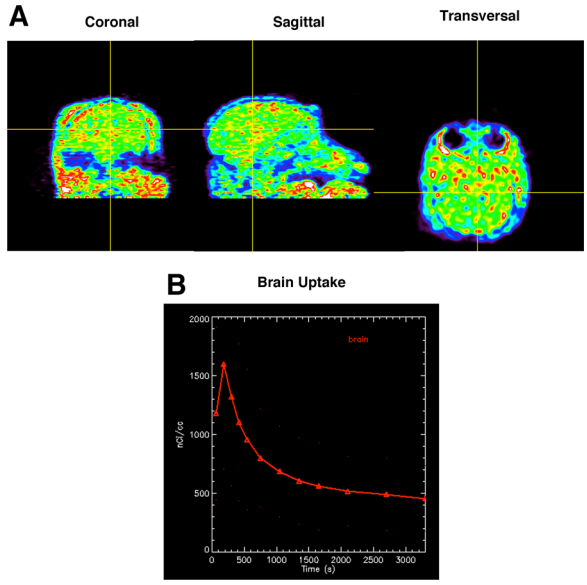

Figure 2. Nonhuman primate microPET images.

Drawing a straightforward region-of-interest (ROI) around the primate brain provided a simple time−activity curve (TAC) for [^{11}C]NML (Figure 2B). From the TAC, [^{11}C]NML uptake in the healthy primate brain was ∼1600 nCi/cc maximum at 3 min followed by rapid egress to 500 nCi/cc. These brain kinetics are similar to other CNS radiopharmaceuticals that we have successfully translated into the clinic (e.g., [^{18}F]FEOBV for imaging the VAChT[30]). Given these promising results, our interest in developing [^{11}C]NML into a radiopharmaceutical for clinical PET imaging of tau NFTs still remained. Therefore, we explored the biodistribution and metabolism profiles of [^{11}C]NML, before turning our attention to evaluation of the specificity of [^{11}C]NML for tau NFTs using in vitro autoradiography.

Metabolism and biodistribution patterns need to be evaluated for any candidate radiopharmaceutical that is being considered for clinical translation. For biodistribution experiments, [^{11}C]NML was injected into anesthetized Sprague−Dawley rats via the tail vein (three per time point), and then, rats were allowed to wake, before being reanesthetized and sacrificed at 5, 30, and 60 min postinjection. Biodistribution confirmed clearance by both the liver and the kidneys, consistent with literature findings for the parent lansoprazole.[31] To investigate metabolism, [^{11}C]NML was injected into anesthetized Sprague−Dawley rats via the tail vein (three per time point), and then, rats were allowed to wake, before being reanesthetized and sacrificed at 5, 15, and 30 min postinjection. Blood was collected at each of the time points and centrifuged to provide plasma fractions, which were analyzed by HPLC and radio-TLC. Analysis demonstrated rapid clearance of [^{11}C]NML from the plasma, consistent with literature data for lansoprazole,[32,33] and revealed the presence of a single polar radioactive metabolite. It is assumed that [^{11}C]NML follows a similar metabolic pathway to that identified for lansoprazole[32,33] and that the polar metabolite is likely to be 5-hydroxy-*N*-methyl lansoprazole or the [^{11}C]NML sulfone derivative. Interestingly, following any of the animal studies reported herein, the charcoal filters on the outlets of the anesthesia

dx.doi.org/10.1021/ml300216t | ACS Med. Chem. Lett. 2012, 3, 936−941

chambers were also discovered to be radioactive. This is indicative of the presence of an exhalable metabolite and is thought to be the result of oxidation of the carbon-11 methyl group to [^{11}C]MeOH or possibly even [^{11}C]CO_2.

Preliminary validation of [^{11}C]NML as a radioligand for tau NFTs was investigated using autoradiography experiments. We have previously developed a line of transgenic rats expressing human tau (hTau +/+, unpublished results). Because of the expense, this line was not sustained, but all brains were harvested upon death of the animal, sliced by microtome, and affixed to microscope slides. The presence of human tau was confirmed by immunocytochemistry (see the Supporting Information), and human tau was clearly present in the cortex and hippocampus of the transgenic hTau +/+ rat brains (Figure 3A) but absent in analogous areas of wild-type (WT) rat brain

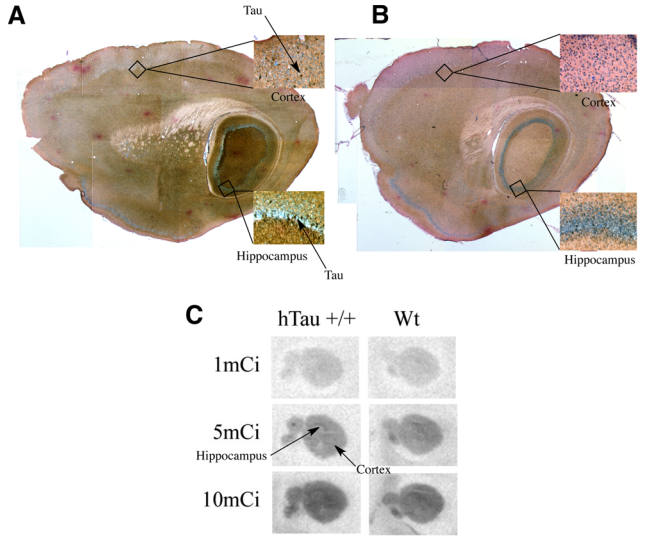

Figure 3. Autoradiography of hTau+/+ and WT rat brain sections with [^{11}C]NML.

slices (Figure 3B). Slices of both the hTau +/+ (n = 3) and the WT (n = 3) brains were incubated with varying amounts of [^{11}C]NML before being rinsed and analyzed with a phosphorescence imager (Figure 3C). While 66 nCi/mL (1 mCi added to 15 mL) and 330 nCi/mL (5 mCi added to 15 mL) images were clear, >660 nCi/mL (10 mCi added to 15 mL) proved too much radioactivity and saturated the image. The images obtained from the lower amounts of radioactivity, however, clearly showed uptake of [^{11}C]NML in the cortical and hippocampal regions, consistent with the immunocytochemistry results. Densitometrical analysis of the images confirmed that uptake was 12% higher in the hTau +/+ cortex and 4% higher in the hTau +/+ hippocampus than the corresponding areas of the WT brains.

Autoradiographical experiments were also conducted using human brain blocks. PSP is a degenerative disorder known to be associated with significant tau pathology.[34] Therefore, a number of PSP cases with tau pathology in the globus pallidus and surrounding regions were selected for investigation (n = 4, age range from 59 to 75). Brain blocks were sliced into 20 μm sections using a cryostat, affixed to slides, and incubated with [^{11}C]NML for 10 min. After this time, slides were washed, dried, and exposed to film for 5 min. The results (Figure 4) show binding of [^{11}C]NML to certain areas of the globus pallidus. Following autoradiography, the slides were subjected

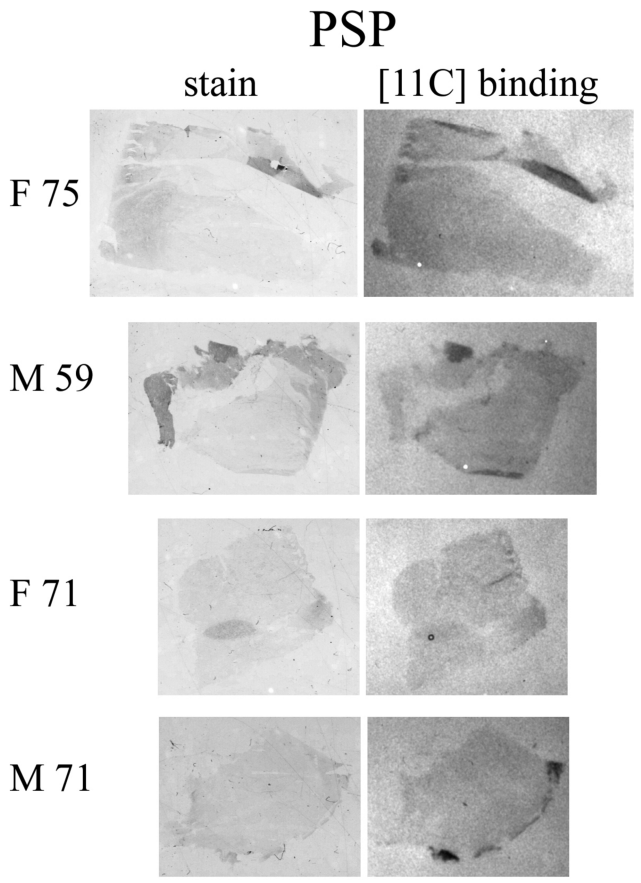

Figure 4. Comparison of [^{11}C]NML binding with Bielschowsky staining in PSP brain sections.

to modified Bielschowsky staining,[35] intended to identify tau NFTs in the PSP brain sections. Figure 4 confirms colocalization of [^{11}C]NML with the Bielschowsky stain, offering further evidence that [^{11}C]NML is binding to tau NFTs.

Finally, confident that [^{11}C]NML has qualitative affinity for tau and potential for in vivo imaging of tau NFT burden in the clinic, attention was turned to quantifying the affinity with saturation binding studies and Scatchard analysis. For lansoprazole, Rojo reported K_i = 2.5 nM against heparin-induced tau filaments and proposed, from docking studies, that the benzimidazole NH formed a key hydrogen bond with the C-terminal hexapeptide (386TDHGAE391) of the tau core.[25] Therefore, it was of critical importance in the present work to determine what effect replacing the NH with N−^{11}CH$_3$ had on the affinity of [^{11}C]NML for tau. Therefore, we conducted binding affinity studies and investigated nonspecific binding (see the Supporting Information) between [^{11}C]NML and analogous heparin-induced tau filaments to those used by Rojo.[25] These studies confirmed K_d and Bmax of [^{11}C]NML against heparin induced tau to be 700 pM and 0.214 fmol/μg, respectively. Thus, replacing the NH with N−^{11}CH$_3$ appears to actually improve the affinity of the scaffold for tau by a factor of 3. It is not immediately obvious why this should be, but perhaps, the methyl group is able to sit in a binding pocket on the protein and improve interactions. Investigations into elucidating the actual binding site are ongoing at this time.

This initial proof-of-concept study has confirmed that lansoprazole is a scaffold of interest for developing a

dx.doi.org/10.1021/ml300216t | ACS Med. Chem. Lett. 2012, 3, 936−941

radiopharmaceutical for quantifying tau NFT burden in vivo using PET imaging. An efficient synthesis of [^{11}C]*N*-methyl lansoprazole has been developed, and preliminary preclinical evaluation suggests that the compound has affinity for tau NFTs. The correlation between NFTs and cognitive decline in AD justifies development of such radiopharmaceuticals, and synthesis of [^{18}F]lansoprazole as well as continuing validation that the scaffold is targeting tau NFTs are ongoing to support these efforts.

■ ASSOCIATED CONTENT

Supporting Information

Full experimental details for compounds synthesized and procedures for radiochemical syntheses, quality control, microPET animal imaging studies, autoradiography, immunocytochemistry, log $P_{oct/water}$ determination, metabolite analyses, and biodistribution studies. This material is available free of charge via the Internet at http://pubs.acs.org.

■ AUTHOR INFORMATION

Corresponding Author

*Tel: +1(734)615-1756. Fax: +1(734)615-2557. E-mail: pjhscott@umich.edu.

Funding

Funding for this research from the University of Michigan Office of the Vice President for Research and the University of Michigan Undergraduate Research Opportunity Program is gratefully acknowledged. The Michigan Alzheimer's Disease Center is funded by Grant #AG08671 and a gift from an anonymous donor.

Notes

The authors declare no competing financial interest.

■ ACKNOWLEDGMENTS

We thank the Michigan Alzheimer's Disease Center for selecting and providing tau-positive brain samples from PSP patients.

■ REFERENCES

(1) Plassman, B. L.; Langa, K. M.; Fisher, G. G.; Heeringa, S. G.; Weir, D. R.; Ofstedal, M. B.; Burke, J. R.; Hurd, M. D.; Potter, G. G.; Rogers, W. L.; Steffens, D. C.; Willis, R. J.; Wallace, R. B. Prevalence of dementia in the United States: the aging, demographics, and memory study. *Neuroepidemiology* **2007**, *29*, 125−132.

(2) Perl, D. P. Neuropathology of Alzheimer's disease. *Mt. Sinai J. Med.* **2010**, *77*, 32−42.

(3) Francis, P. T.; Palmer, A. M.; Snape, M.; Wilcock, G. K. The cholinergic hypothesis in Alzheimer's disease: A review of progress. *J. Neurol. Neurosurg. Psychiatry* **1999**, *66*, 137−147.

(4) For a review see Zeman, M. N.; Carpenter, G. M.; Scott, P. J. H. Diagnosis of dementia using nuclear medicine imaging modalities. In *12 Chapters on Nuclear Medicine*; Gholamrezanezhad, A., Ed.; In Tech: Croatia, 2011; pp 199−230.

(5) Morais, G. R.; Paulo, A.; Santos, I. A synthetic overview of radiolabeled compounds for β-amyloid imaging. *Eur. J. Org. Chem.* **2012**, 1279−1293.

(6) Nordberg, A. PET Imaging of amyloid in Alzheimer's disease. *Lancet Neurol.* **2004**, *3*, 519−527.

(7) Nordberg, A. Amyloid imaging in Alzheimer's disease. *Neuropsychologia* **2008**, *46*, 1636−1641.

(8) Herholz, K.; Ebmeier, K. Clinical amyloid imaging in Alzheimer's disease. *Lancet Neurol.* **2011**, *10*, 667−670.

(9) Karran, E.; Mercken, M.; De Strooper, B. The amyloid cascade hypothesis for Alzheimer's disease: an appraisal for the development of therapeutics. *Nat. Rev. Drug Discovery* **2011**, *10*, 698−712.

(10) Hardy, J.; Selkoe, D. J. The amyloid hypothesis of Alzheimer's disease: Progress and problems on the road to therapeutics. *Science* **2002**, *297*, 353−356.

(11) Klunk, W. E.; Engler, H.; Nordberg, A.; Wang, Y.; Blomqvist, G.; Holt, D. P.; Bergström, M.; Savitcheva, I.; Huang, G. F.; Estrada, S.; Ausén, B.; Debnath, M. L.; Barletta, J.; Price, J. C.; Sandell, J.; Lopresti, B. J.; Wall, A.; Koivisto, P.; Antoni, G.; Mathis, C. A.; Långstrom, B. Imaging brain amyloid in Alzheimer's disease with Pittsburgh compound-B. *Ann. Neurol.* **2004**, *55*, 306−319.

(12) Vandenberghe, R.; Van Laere, K.; Ivanoiu, A.; Salmon, E.; Bastin, C.; Triau, E.; Hasselbalch, S.; Law, I.; Andersen, A.; Korner, A.; Minthon, L.; Garraux, G.; Nelissen, N.; Bormans, G.; Buckley, C.; Owenius, R.; Thurfjell, L.; Farrar, G.; Brooks, D. J. 18F-Flutemetamol amyloid imaging in Alzheimer disease and mild cognitive impairment: A phase 2 trial. *Ann. Neurol.* **2010**, *68*, 319−329.

(13) Wong, D. F.; Rosenberg, P. B.; Zhou, Y.; Kumar, A.; Raymont, V.; Ravert, H. T.; Dannals, R. F.; Nandi, A.; Brašić, J. R.; Ye, W.; Hilton, J.; Lyketsos, C.; Kung, H. F.; Joshi, A. D.; Skovronsky, D. M.; Pontecorvo, M. J. In vivo imaging of amyloid deposition in Alzheimer disease using the radioligand ^{18}F-AV-45 (Florbetapir F 18). *J. Nucl. Med.* **2010**, *51*, 913−920.

(14) Rowe, C. C.; Ackerman, U.; Browne, W.; Mulligan, R.; Pike, K. L.; O'Keefe, G.; Tochon-Danguy, H.; Chan, G.; Berlangieri, S. U.; Jones, G.; Dickinson-Rowe, K. L.; Kung, H. P.; Zhang, W.; Kung, M. P.; Skovronsky, D.; Dyrks, T.; Holl, G.; Krause, S.; Friebe, M.; Lehman, L.; Lindemann, S.; Dinkelborg, L. M.; Masters, C. L.; Villemagne, V. L. Imaging of amyloid β in Alzheimer's disease with ^{18}F-BAY94-9172, a novel PET tracer: proof of mechanism. *Lancet Neurol.* **2008**, *7*, 129−135.

(15) Rowe, C. C.; Villemagne, V. L. Brain amyloid imaging. *J. Nucl. Med.* **2011**, *52*, 1733−1740.

(16) Clark, C. M.; Schneider, J. A.; Bedell, B. J.; Beach, T. G.; Bilker, W. B.; Mintun, M. A.; Pontecorvo, M. J.; Hefti, F.; Carpenter, A. P.; Fllitter, M. L.; Krautkramer, M. J.; Kung, H. F.; Coleman, R. E.; Doraiswamy, P. M.; Fleisher, A. S.; Sabbagh, M. N.; Sadowsky, C. H.; Reiman, E. M.; Zehntner, S. P.; Skovronsky, D. M. for the AV45-A07 Study Group. Use of florbetapir-PET for imaging β-amyloid pathology. *J. Am. Med. Assoc.* **2011**, *305*, 275−283.

(17) Wolk, D. A.; Grachev, I. D.; Buckley, C.; Kazi, H.; Grady, M. S.; Trojanowski, J. Q.; Hamilton, R. H.; Sherwin, P.; McLain, R.; Arnold, S. E. Association between in vivo fluorine 18-labeled flutemetamol amyloid positron emission tomography imaging and in vivo cerebral cortical histopathology. *Arch. Neurol.* **2011**, *68*, 1398−1403.

(18) Giannakopoulos, P.; Herrmann, F. R.; Bussière, T.; Bouras, C.; Kövari, E.; Perl, D. P.; Morrison, J. H.; Gold, G.; Hof, P. R. Tangle and neuron numbers, but not amyloid load, predict cognitive status in Alzheimer's disease. *Neurology* **2003**, *60*, 1495−1500.

(19) Ludolph, A. C.; Kassubek, J.; Landwehrmeyer, B. G.; Mandelkow, E.; Mandelkow, E.-M.; Burn, D. J.; Caparros-Lefebvre, D.; Frey, K. A.; de Yebenes, J. G.; Gasser, T.; Heutink, P.; Höglinger, G.; Jamrozik, Z.; Jellinger, K. A.; Kazantsev, A.; Kretzschmar, H.; Lang, A. E.; Litvan, I.; Lucas, J. J.; McGeer, P. L.; Melquist, S.; Oertel, W.; Otto, M.; Paaviour, D.; Reum, T.; Saint-Raymond, A.; Steele, J. C.; Tolnay, M.; Tumani, H.; van Swieten, J. C.; Vanier, M. T.; Vonsattel, J.-P.; Wagner, S.; Wszolek, Z. K. for the Reisensburg Working Group for Tauopathies with Parkinsonism. Tauopathies with parkinsonism: clinical spectrum, neuropathologic basis, biological markers, and treatment options. *Eur. J. Neurol.* **2009**, *16*, 297−309.

(20) Okamura, N.; Suemoto, T.; Furumoto, S.; Suzuki, M.; Shimadzu, H.; Akatsu, H.; Yamamoto, T.; Fujiwara, H.; Nemoto, M.; Maruyama, M.; Arai, H.; Yanai, K.; Sawada, T.; Kudo, Y. Quinoline and benzimidazole derivatives: Candidate probes for in vivo imaging of tau pathology in Alzheimer's disease. *J. Neurosci.* **2005**, *25*, 10857−10862.

(21) Fodero-Tavoletti, M. T.; Okamura, N.; Furumoto, S.; Mulligan, R. S.; Connor, A. R.; McLean, C. A.; Cao, D.; Rigopoulos, A.;

Cartwright, G. A.; O'Keefe, G.; Gong, S.; Adlard, P. A.; Barnham, K. J.; Rowe, C. C.; Masters, C. L.; Kudo, Y.; Cappai, R.; Yanai, K.; Villemagne, V. L. ^{18}F-THK523: a novel in vivo tau imaging ligand for Alzheimer's disease. *Brain* **2011**, *134*, 1089−1100.
(22) Villemagne, V. L.; Furumoto, S.; Fodero-Tavoletti, M. T.; Mulligan, R. S.; Hodges, J.; Kudo, Y.; Masters, C. L.; Yanai, K.; Rowe, C. C.; Okamura, N. In vivo tau imaging in Alzheimer's disease. *J. Nucl. Med.* **2012**, *53* (Suppl. 1), 11P.
(23) Zhang, W.; Arteaga, J.; Cashion, D. K.; Chen, G.; Gangadharmath, U.; Gomez, L. F.; Kasi, D.; Lam, C.; Liang, Q.; Liu, C.; Mocharla, V. P.; Mu, F.; Sinha, A.; Szardenings, A. K.; Wang, E.; Walsh, J. C.; Xia, C.; Yu, C.; Zhao, T.; Kolb, H. C. A Highly Selective and Specific PET Tracer for Imaging of Tau Pathologies. *J. Alzheimers Dis.* **2012**, *31*, 601−612.
(24) Small, G. W.; Kepe, V.; Ercoli, L. M.; Siddarth, P.; Bookheimer, S. Y.; Miller, K. J.; Lavretsky, H.; Burggren, A. C.; Cole, G. M.; Vinters, H. V.; Thompson, P. M.; Huang, S. C.; Satyamurthy, N.; Phelps, M. E.; Barrio, J. R. PET of brain amyloid and tau in mild cognitive impairment. *N. Engl. J. Med.* **2006**, *355*, 2652−2663.
(25) Rojo, L. E.; Alzate-Morales, J.; Saavedra, I. N.; Davies, P.; Maccioni, R. B. Selective interaction of lansoprazole and astemizole with tau polymers: Potential new clinical use in diagnosis of Alzheimer's disease. *J. Alzheimers Dis.* **2010**, *19*, 573−589.
(26) Shao, X.; Hoareau, R.; Runkle, A. C.; Tluczek, L. J. M.; Hockley, B. G.; Henderson, B. D.; Scott, P. J. H. Highlighting the versatility of the TRACERlab synthesis modules. Part 2: Fully automated production of [^{11}C]-labeled radiopharmaceuticals using a TRACERlab FXc-pro. *J. Labelled Compd. Radiopharm.* **2011**, *54*, 819−838.
(27) Shin, J. M.; Cho, Y. M.; Sachs, G. Chemistry of Covalent Inhibition of the Gastric (H^+, K^+)-ATPase by Proton Pump Inhibitors. *J. Am. Chem. Soc.* **2004**, *126*, 7800−7811.
(28) Sarkadi, B.; Homolya, L.; Szakács, G.; Váradi, A. Human multidrug resistance ABCB and ABCG transporters: Participation in a chemoimmunity defense system. *Physiol. Rev.* **2006**, *86*, 1179−1236.
(29) Blanckaert, P.; Burvenich, I.; Staelens, S.; De Bruyne, S.; Moerman, L.; Wyffels, L.; De Vos, F. Effect of cyclosporin A administration on the biodistribution and multipinhole μSPECT imaging of [^{123}I]R91150 in rodent brain. *Eur. J. Nucl. Med. Mol. Imaging* **2009**, *36*, 446−453.
(30) Petrou, M.; Koeppe, R. A.; Scott, P. J. H.; Bohnen, N. I.; Kilbourn, M. R.; Frey, K. PET Imaging of the vesicular acetylcholine transporter. *J. Nucl. Med.* **2012**, *53* (Suppl. 1), 89P.
(31) Karol, M. D.; Machinist, J. M.; Cavanaugh, J. M. Lansoprazole pharmacokinetics in subjects with various degress of kidney function. *Clin. Pharmacol. Ther.* **1997**, *61*, 450−458.
(32) Kim, K.-A.; Kim, M.-J.; Park, J.-Y.; Shon, J.-H.; Yoon, Y.-R.; Lee, S.-S.; Liu, K.-H.; Chun, J.-H.; Hyun, M.-H.; Shin, J.-G. Stereoselective metabolism of lansoprazole by human liver cytochrome P450 enzymes. *Drug Metab. Dispos.* **2003**, *31*, 1227−1234.
(33) Pearce, R. E.; Rodrigues, A. D.; Goldstein, J. A.; Parkinson, A. Identification of the human P450 enzymes involved in lansoprazole metabolism. *J. Pharmacol. Exp. Ther.* **1996**, *277*, 805−816.
(34) Williams, D. R.; Holton, J. L.; Strand, C.; Pittman, A.; de Silva, R.; Lees, A. J.; Revesz, T. Pathological tau burden and distribution distinguishes progressive supranuclear palsy-parkinsonism from Richardson's syndrome. *Brain* **2007**, *130*, 1566−1576.
(35) Anderson, J. M.; Hampton, D. W.; Patani, R.; Pryce, G.; Crowther, R. A.; Reynolds, R.; Franklin, R. J.; Giovannoni, G.; Compston, D. A.; Baker, D.; Spillantini, M. G.; Chandran, S. Abnormally phosphorylated tau is associated with neuronal and axonal loss in experimental autoimmune encephalomyelitis and multiple sclerosis. *Brain* **2008**, *131*, 1736−1748.